

commodating fumagillin's side chain in the specificity pocket. In MetAP-1, the size of the conserved Phe<sup>177</sup> (HsIle<sup>338</sup>) makes the pocket substantially narrower (Figs. 2 and 4C). The relatively slim side chain of methionine can be accommodated in this narrower pocket whereas the bulky and conformationally restricted side chain of fumagillin cannot. Because MetAP-1 lacks Tyr<sup>444</sup> and has an open specificity pocket, the narrower pocket would be easily accessible. Thus, fumagillin's inability to inhibit MetAP-1 can be traced to the position of the nucleophilic His in MetAP-1, the difficulty of repositioning this residue because of consistent size differences in the adjacent residues, and a narrowing of the specificity pocket.

Our results provide a structural framework for understanding the relation of human MetAP-2 to prokaryotic and other eukaryotic MetAPs, fumagillin's ability to inhibit MetAP-2, and the basis of fumagillin's specificity. Insights from this analysis will also be useful in structure-based drug design. Fumagillin-based therapeutics such as TNP-470 share fumagillin's conformationally rigid template and key features. The two drugs differ in the side chain at C6, a region that shows few, if any, ligand interactions. Thus, TNP-470 is likely to inhibit MetAP-2 by occupying the active site in the same fashion as fumagillin.

#### References and Notes

1. J. Folkman, *Nature Med.* **1**, 27 (1995).
2. M. McCowen, M. Callender, J. F. Lawlis Jr., *Science* **113**, 202 (1951); F. R. Hanson and T. E. Eble, *J. Bacteriol.* **58**, 527 (1949).
3. D. Ingber et al., *Nature* **348**, 555 (1990).
4. B. J. Dezube et al., *J. Clin. Oncol.* **16**, 1444 (1998); Y. Kawarada et al., *Pancreas* **15**, 251 (1997); H. Konno et al., *Cancer* **77**, 1736 (1996); Y. Ohta et al., *Br. J. Cancer* **75**, 512 (1997); Y. Singh et al., *Breast Cancer Res. Treat.* **45**, 15 (1997); E. Wassberg and R. Christofferson, *Eur. J. Cancer* **33**, 2020 (1997); J. L. Xia et al., *J. Cancer Res. Clin. Oncol.* **123**, 383 (1997); P. Twardowski and W. J. Gradishar, *Curr. Opin. Oncol.* **9**, 584 (1997).
5. N. Sin et al., *Proc. Natl. Acad. Sci. U.S.A.* **94**, 6099 (1997).
6. E. C. Griffith et al., *Chem. Biol.* **4**, 461 (1997).
7. J. Wang, N. Quan, J. Henkin, *Proc. Am. Assoc. Cancer Res.* **39**, 98 (abstr.) (1998).
8. S. M. Arfin et al., *Proc. Natl. Acad. Sci. U.S.A.* **92**, 7714 (1995).
9. The entire HsMetAP-2 reading frame was excised from pBluescript and inserted into the pACSG2 baculovirus transfer vector (PharMingen, San Diego). This plasmid was cotransfected with BacVector-3000 (Novagen, Milwaukee, WI) into Sf9 cells. The virus was cloned and the protein expressed in Sf21 cells grown in Cyto-SF9 medium (Kemp Biotechnologies, Frederick, MD). A cell pellet from 2.5 liters of culture was lysed in 100 ml of 20 mM Hepes (pH 7.4), 150 mM NaCl, 10% glycerol, and protease inhibitors. The lysate was centrifuged at 48,000g for 1 hour, and two volumes of 10 mM Hepes (pH 7.4) were added to the supernatant. The material was applied to an SP-Sepharose (Pharmacia) column equilibrated with 10 mM Hepes. The column was washed with the Hepes containing 100 mM NaCl, and the proteins were eluted with a linear gradient from 100 to 500 mM NaCl in Hepes buffer. Fractions with MetAP-2 were combined and dialyzed against 100 mM potassium phosphate, pH 7.0, and applied to a hydroxylapatite

(Bio-Rad, CHT type 1) column equilibrated with the same buffer. Proteins were eluted with a linear gradient from 100 to 400 mM potassium phosphate, pH 7.0. We obtained more than 20 mg of pure MetAP-2 per liter of culture. Mass spectroscopy gave a molecular weight of 53,060, and the NH<sub>2</sub>-terminus appeared to be blocked. The protein was stored at 4°C in 10 mM Hepes, 10% glycerol, 150 mM NaCl, and 1 mM CoCl<sub>2</sub>.

10. Crystals of HsMetAP-2 were grown in 1 to 2 weeks at 4°C from sitting drops, with a protein concentration of 12 mg/ml in 10 mM Hepes (pH 7.2), 10% glycerol, and 100 mM NaCl. The reservoir solution contained 15 to 30% *t*-butanol in 33 to 100 mM sodium citrate buffer, pH 5.2 to 5.6. The crystals belong to the orthorhombic space group C22<sub>2</sub>1 with  $a = 90.49$  Å,  $b = 99.38$  Å, and  $c = 101.59$  Å and contain one molecule in the asymmetric unit. HsMetAP-2-fumagillin complex crystals were prepared by adding 1 μl of 50 mM fumagillin (ethanol) directly into a crystallization drop and equilibrated for 12 hours before mounting.
11. We collected data for both MetAP-2 and its fumagillin complex to a resolution of 1.8 Å (154,879 and 158,945 measurements of 42,194 and 40,944 unique reflections, 98.8% and 94.7% completeness, 3.7 and 3.9 redundancy, and  $R_{\text{sym}}$  values of 0.069 and 0.078, respectively) at the F1 station of CHESS (Cornell High-Energy Synchrotron Source) using 0.922 Å radiation ( $R_{\text{sym}} = \sum |I - \langle I \rangle| / \sum \langle I \rangle$ , where  $I$  is the integrated intensity of a given reflection). Phases were obtained by the molecular replacement technique as implemented in AMoRe [J. Navaza, *Acta Crystallogr. Sect. D Biol. Crystallogr.* **50**, 157 (1994)] and the 1.75 Å resolution model of PfMetAP-2 (13), Protein Data Bank accession code 1XGS. Extensive model building with O [T. A. Jones, J. Y. Zou, S. W. Cowan, M. Kjeldgaard, *Acta Crystallogr. Sect. A* **47**, 110 (1991)] and rigid body and restrained refinement with X-PLOR [A. T. Brünger, J. Kuriyan, M. Karplus, *Science* **235**, 458 (1987)] and REFMAC [G. N. Murshudov, A. A. Vagin, E. J. Dodson, *Acta Crystallogr. Sect. D Biol. Crystallogr.* **53**, 240 (1997)] brought the conventional  $R$  and  $R_{\text{free}}$  (calculated for 7% and 5% of the data not used for the refinement of native and complex, respectively) below 0.20 and 0.25, respectively. At this stage in the structure of the fumagillin complex, a fumagillin model could easily be built into the well-defined difference electron density map. The current models include 355 residues (110 through 138 and 153 through 478), two cobalt atoms, 240 waters, and two *t*-butanols for the native structure. In the complex structure, there are 203 waters, no *t*-butanols, and 33 fumagillin atoms. The current  $R$  values from 25.0 to 1.8 Å are 0.183 and 0.194 for the native and complex structures (0.228 and 0.231 for  $R_{\text{free}}$ ). The root mean square deviations from ideal bond lengths and bond angles are 0.012 Å and 2.2°.
12. S. L. Roderick and B. W. Matthews, *Biochemistry* **32**, 3907 (1993).
13. T. H. Tahirov et al., *J. Struct. Biol.* **121**, 68 (1998).
14. J. Kraut, *Annu. Rev. Biochem.* **46**, 331 (1977).
15. R. L. Kendall and R. A. Bradshaw, *J. Biol. Chem.* **267**, 20667 (1992).
16. X. Li and Y.-H. Chang, *Proc. Natl. Acad. Sci. U.S.A.* **92**, 12357 (1995).
17. G. J. Barton, *Protein Eng.* **6**, 37 (1993).
18. P. J. Kraulis, *J. Appl. Cryst.* **24**, 946 (1991).
19. A. C. Wallace, R. Laskowski, J. Thornton, *Protein Eng.* **8**, 127 (1995).
20. We thank R. Gillilan for graphics, the MacCHESS staff for help with data collection, J. Liu for helpful discussions, and Y.-H. Chang for the HsMetAP-2 pBluescript plasmid. The Cornell work was funded in part by U.S. Public Health Service grants CA59021 and CA24487 (to J.C.). C.M.C. is a Donaghue Foundation New Investigator. Atomic coordinates have been deposited in the Protein Data Bank under accession numbers 1BN5 (HsMetAP-2) and 1BOA (HsMetAP-2-fumagillin).

7 August 1998; accepted 7 October 1998

## A Structural Explanation for the Recognition of Tyrosine-Based Endocytotic Signals

David J. Owen and Philip R. Evans\*

Many cell surface proteins are marked for endocytosis by a cytoplasmic sequence motif, tyrosine-X-X-(hydrophobic residue), that is recognized by the μ2 subunit of AP2 adaptors. Crystal structures of the internalization signal binding domain of μ2 complexed with the internalization signal peptides of epidermal growth factor receptor and the trans-Golgi network protein TGN38 have been determined at 2.7 angstrom resolution. The signal peptides adopted an extended conformation rather than the expected tight turn. Specificity was conferred by hydrophobic pockets that bind the tyrosine and leucine in the peptide. In the crystal, the protein forms dimers that could increase the strength and specificity of binding to dimeric receptors.

The localization and movement of compartment-specific proteins within the cell is largely achieved through the recognition of short sequence motifs by targeting proteins. One of the most studied processes involving such signal recognition is clathrin-mediated endocytosis,

which occurs in vesicle trafficking and the internalization of nutrient and growth factor receptors when bound to their appropriate cargo molecules [reviewed in (1)]. During the internalization of activated growth factor receptors such as the epidermal growth factor receptor (EGFR) tyrosine kinase [reviewed in (2)], receptors are removed from the cell surface in clathrin-coated vesicles and ultimately directed to the endosome and lysosome, where they are inactivated by proteolytic degradation (3, 4).

Medical Research Council Laboratory of Molecular Biology, Hills Road, Cambridge CB2 2QH, UK.

\*To whom correspondence should be addressed. E-mail: pre@mrc-lmb.cam.ac.uk

The first stage of endocytosis is the formation of a clathrin-coated pit, when mechanical invagination of a patch of membrane by clathrin occurs as it forms a polyhedral lattice, as does the preferential sorting of selected transmembrane proteins into the pits by adaptor complexes (APs). At least three similar AP complexes (AP1, AP2, and AP3) have been identified and appear to be associated with different cell compartments. The APs comprise four types of subunit: two large (~100 kD) ( $\alpha$  and  $\beta$ 2 in AP2), one medium (~50 kD) ( $\mu$ 2 in AP2), and one small (~17 kD) ( $\sigma$ 2 in AP2). AP2 adaptors link the proteins to be endocytosed (via the  $\mu$ 2 subunit) with the nascent clathrin coat (via the  $\alpha$  and  $\beta$ 2 subunits), and via the  $\alpha$  subunit, they recruit the components (such as EPS15, amphiphysin, and dynamin) needed to drive and regulate the formation of clathrin-coated vesicles [reviewed in (5, 6)]. The short linear sequence motifs that act as internalization signals mainly fall into two classes. The first, and most common, contains a critical tyrosine residue, and members of this group mostly conform to the consensus sequence Yxx $\emptyset$  [where  $\emptyset$  is a bulky hydrophobic residue (Leu, Ile, Met, or Phe) (7)] that binds directly to  $\mu$ 2 subunits (8); the second is the "dileucine" motif DxxxLL (9), which interacts with the  $\beta$ 1 subunit of AP1 (10) but may also bind indirectly to the  $\mu$  subunit via an "adaptor" protein (11, 12).

To investigate the nature and selectivity of the binding of Yxx $\emptyset$  internalization signals to APs, we have solved the crystal structures to 2.7 Å resolution of the signal binding domain of  $\mu$ 2 (residues 158 to 435) (13) complexed with the internalization signal peptides from EGFR (FYRALM) (14) and TGN38 (DYQRLN) (15, 16). The protein has an elongated, banana-shaped, all  $\beta$ -sheet structure. It can be considered as two  $\beta$ -sandwich subdomains (A and B), with subdomain B inserted between strands 6 and 15 of subdomain A, and joined edge to edge such that the convex surface is a continuous nine-stranded mixed  $\beta$  sheet that runs the whole length of the molecule (Figs. 1 and 2).

The two peptides bind in an identical manner to a site on the surface of two parallel  $\beta$ -sheet strands ( $\beta$ 1 and  $\beta$ 16) in subdomain A (Fig. 3). The peptide assumes an extended conformation when bound, not a tight  $\beta$  turn as has been proposed (17). Hydrophobic pockets exist for the binding of both the tyrosine and the  $\emptyset$  residue on either side of edge strand  $\beta$ 16. These pockets are positioned such that when the side chains of the target peptide are correctly bound, three additional hydrogen bonds are made between the backbone of the peptide and  $\beta$ -strand 16, forming an extra strand on the inner edge of the nine-stranded  $\beta$  sheet (represented schematically in Fig. 3C). A similar mechanism of increased strength of binding through  $\beta$ -strand formation on correct recognition of key side chains has been demonstrated in a number of

cases, including the interactions of protein kinases with their substrates (18) and protein phosphatases with their regulatory subunits (19).

The tyrosine residue of the internalization peptide makes extensive interactions with side chains in its binding pocket. There are hydrophobic interactions between the tyrosine ring and Trp<sup>421</sup> and Phe<sup>174</sup> as well as stacking on the guanidinium group of Arg<sup>423</sup>. The hydroxyl group of the tyrosine participates in a network of hydrogen bonds with Asp<sup>176</sup>, Lys<sup>203</sup> (from  $\beta$ 2), and again Arg<sup>423</sup>, explaining why a Phe at this position gives only poor binding (20). As well as contributing directly to the strength of binding via a direct hydrogen bond to the tyrosine OH, Asp<sup>176</sup> appears to play an important role in correctly orienting the guanidinium group of Arg<sup>423</sup>. The critical role of Asp<sup>176</sup> is reflected in its absolute conservation among all  $\mu$ 2,  $\mu$ 1, and  $\mu$ 3 sequences (Fig. 1C). The other major determinant, as defined by sequence and combinatorial peptide library analysis of internalization signals, is the presence of a bulky hydrophobic residue at the Y+3 position (7). The binding site for this residue is a cavity lined with aliphatic residues (Fig. 3B). The size and flexibility of the side chains within this pocket would allow for the accommodation of any of

the residues (Leu, Phe, Met, Ile) that are possible at this position.

Peptide library screening has revealed a preference for an arginine residue at either Y+2 (strong) or Y+1 (weak) (7). In the DYQRLN (TGN38) complex, the arginine forms hydrophobic interactions mainly with Trp<sup>421</sup> but also with Ile<sup>419</sup> (Fig. 3), with its guanidinium group exposed to solvent and making a hydrogen bond between Ne and the carbonyl of Lys<sup>420</sup> (Fig. 2B): The favorable hydrophobic interaction outweighs the unfavorable electrostatic interaction with the marked positive potential of the peptide binding surface (Fig. 4, C and D). The FYRALM (EGFR) peptide contains an arginine at the Y+1 position that is not well ordered, implying that it has no significant interaction with  $\mu$ 2. The nature and disposition of the pockets explains why the dileucine type of internalization motif is unable to bind to  $\mu$ 2, because there would be no residue capable of filling the tyrosine binding pocket. It also indicates that if the low density lipoprotein receptor internalization signal NPVY does bind weakly to  $\mu$ 2 (7) and not via an adaptor protein, it would have to do so in the reverse orientation, that is, with its Asn residue in the Y+3 pocket.

Src homology region 2 (SH2) domains bind similar Yxx $\emptyset$  motifs in an extended conforma-

**Table 1.** Statistics on data collection and phasing. Data collection values in parentheses are for the high-resolution shell.

	Native	Xe	EMTS	FYRALM peptide complex	DYQRLN peptide complex
Protein construct	122-435	122-435	122-435	122-435	158-435
	<i>Data collection</i>				
Resolution (Å) (outer bin)	3.0 (3.16)	3.0 (3.16)	4.0 (4.22)	2.65 (2.79)	2.70 (2.85)
$R_{\text{merge}}^*$	0.101 (0.910)	0.079 (0.851)	0.116 (0.302)	0.089 (0.882)	0.101 (1.47)
$\langle\langle I \rangle\rangle / \langle\langle I \rangle\rangle$	17.3 (2.9)	25.9 (2.2)	20.2 (7.2)	21.3 (2.1)	23.5 (2.2)
Completeness (%)	99.9 (99.9)	99.8 (99.8)	99.7 (100)	99.4 (96.7)	98.4 (99.8)
Multiplicity	10.9 (10.6)	10.7 (8.2)	10.4 (10.6)	9.2 (8.1)	15.8 (14.7)
$R_{\text{meas}}^\dagger$	0.106 (0.957)	0.088 (0.985)	0.124 (0.334)	0.094 (0.942)	0.104 (1.52)
Wilson plot $B$ (Å <sup>2</sup> )	100			85	78
	<i>Multiple isomorphous replacement phasing</i>				
Number of sites		1	8		
$R_{\text{deriv}}^\ddagger$		0.096	0.255		
$R_{\text{cullis}}^\S$ : acentric (centric)§		0.643 (0.707)	0.662 (0.683)		
Phasing power: acentric (centric)		1.88 (1.19)	2.29 (1.87)		
Anomalous phasing power		0.54	2.28		
Mean figure of merit: acentric (centric)	0.374 (0.350)			0.187 (0.205)¶	
Figure of merit after solvent flattening (all data)	0.864			0.849¶	
	<i>Refinement</i>				
$R$ ( $R_{\text{free}}^\#$ )#				0.273 (0.297)	0.282 (0.325)
$B$ (Å <sup>2</sup> )				60	75
$N_{\text{reflections}}$ ( $N_{\text{free}}$ )				19,296 (842)	18,413 (801)
$N_{\text{atoms}}$ ( $N_{\text{water}}$ )				2143 (51)	2143 (50)
rmsd bond length (Å)				0.010	0.012
rmsd angle distance (Å)				0.038	0.040

\* $R_{\text{merge}} = \sum_i |I_h - I_{h,i}| / \sum_i I_h$ , where  $I_h$  is the mean intensity for reflection  $h$ .  $\dagger R_{\text{meas}} = \sum \sqrt{(n/n-1)} \sum_i |I_h - I_{h,i}| / \sum_i I_h$ , the multiplicity-weighted  $R_{\text{merge}}$  (34).  $\ddagger R_{\text{deriv}} = \sum |F_{\text{PH}} - F_p| / \sum F_p$ .  $\S R_{\text{cullis}} = \sum |F_{\text{PH}} - F_p| - |F_{\text{H(calc)}}| / \sum |F_{\text{PH}} - F_p|$ .  $\|$  Phasing power =  $\langle |F_{\text{H(calc)}}| \rangle / \langle \text{phase-integrated lack of closure} \rangle$ .  $\¶$  Phasing using the FYRALM complex data as native.  $\#R = \sum |F_p - F_{\text{calc}}| / \sum F_p$ .

REPORTS

tion, with the tyrosine phosphorylated (21, 22), but there is no homology either in the structure of the proteins or in their mode of binding. In the case of SH2 domains, the specificity and strength of binding to the target peptide arise predominantly from ionic interactions with the phosphate moiety. The structure of the complex demonstrates that if the tyrosine residue were to be phosphorylated, it would be incapable of binding to  $\mu_2$ , both because the size of the tyrosine pocket is too small and because Asp<sup>176</sup> would repel the phosphate. This is supported by data suggesting that phosphorylated peptides will not bind to  $\mu_2$  subunit (20) and that phosphorytyrosine cannot displace EGFR that is bound to AP2 (23).

The residues involved in signal recognition are conserved in  $\mu_2$  subunits from all species (Fig. 1C). The binding sites in the  $\mu_1$  subunit of AP1 (AP47) are also very similar, although the change Lys<sup>420</sup> → Pro may alter the specificity for the Y+3 residue. In the AP3 homolog ( $\mu_3A$  or p47A), the residues Lys<sup>203</sup> and Arg<sup>423</sup> in  $\mu_2$  involved in binding the tyrosine of the Yxx $\Phi$  motif are replaced by Cys and Lys, respectively, which would be expected to reduce the affinity for tyrosine signals to  $\mu_3A$ . The substitutions Leu<sup>173</sup> → Ala and Leu<sup>175</sup> → Phe in the Y+3 pocket (Fig. 1C) may alter the selectivity for residues at this position. The exchange of Trp<sup>421</sup> in  $\mu_2$  for a glycine in  $\mu_3A$  would remove the specificity for an arginine at the Y+2 position.

How does the machinery of endocytosis recognize a relatively nonspecific signal such as the sequence Yxx $\Phi$ ? One possibility arises from the observation that most receptors are internalized as dimers, often induced by ligand binding on the outside of the cell, which could

place two internalization signals adjacent to each other. Recognition of this dimer would increase the avidity of binding, relative to the monomer, without necessarily precluding binding of monomeric receptors. In the crystal structure, the  $\mu_2$  molecules form a dimer around a crystallographic twofold axis, placing the internalization signal peptides close to each other in a large groove (Fig. 4). The dimer buries 1100 Å<sup>2</sup> of accessible surface, which is

smaller than most stable dimer interfaces (typically at least 1200 Å<sup>2</sup>), but  $\mu_2$  is only a small part of the whole AP2 molecule, and additional interactions may be formed between other subunits of AP2 in a dimer. This provides an attractive explanation for the recognition of dimeric receptors, particularly as peptide binding would favor dimerization because the peptide contributes 17% of the interface. Dimerization of

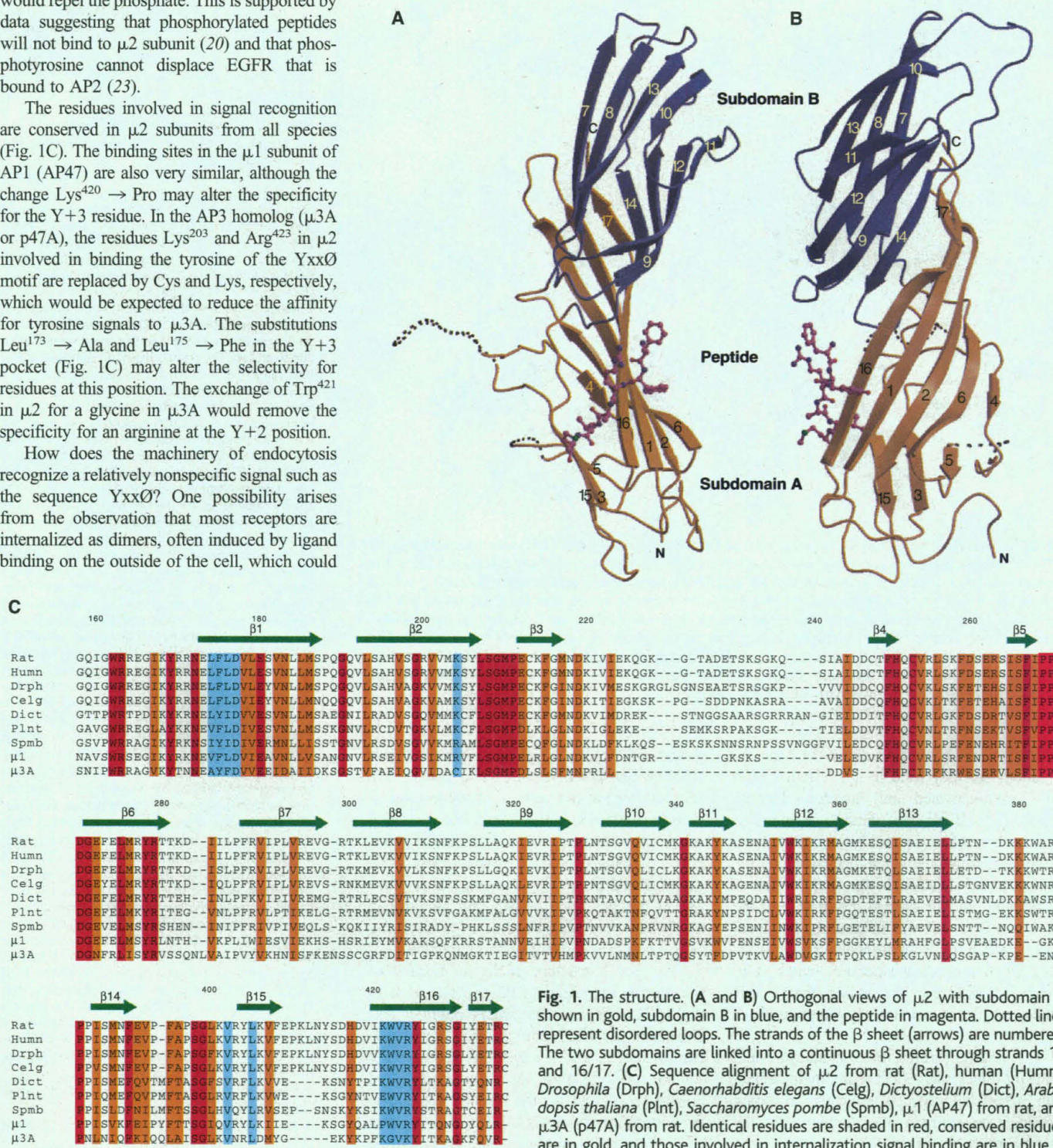


**Fig. 1.** The structure. (A and B) Orthogonal views of  $\mu_2$  with subdomain A shown in gold, subdomain B in blue, and the peptide in magenta. Dotted lines represent disordered loops. The strands of the  $\beta$  sheet (arrows) are numbered. The two subdomains are linked into a continuous  $\beta$  sheet through strands 14 and 16/17. (C) Sequence alignment of  $\mu_2$  from rat (Rat), human (Humn), *Drosophila* (Drph), *Caenorhabditis elegans* (Celg), *Dictyostelium* (Dict), *Arabidopsis thaliana* (Plnt), *Saccharomyces pombe* (Spmb),  $\mu_1$  (AP47) from rat, and  $\mu_3A$  (p47A) from rat. Identical residues are shaded in red, conserved residues are in gold, and those involved in internalization signal binding are in blue.

REPORTS

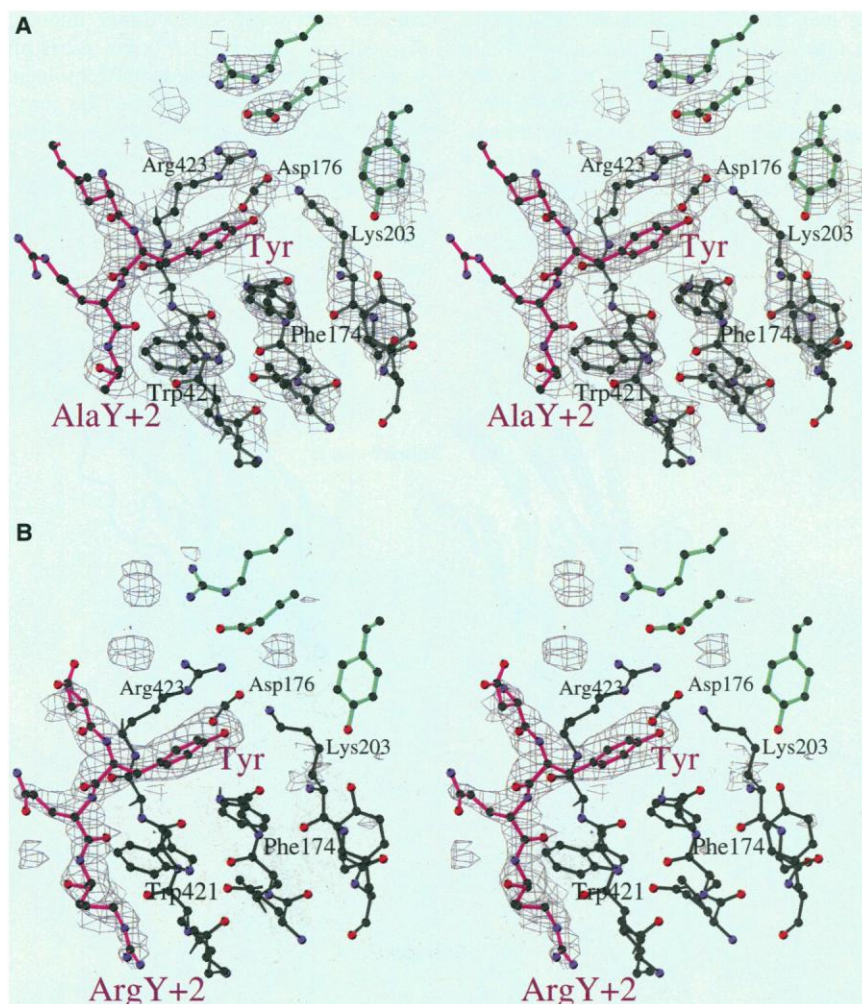


**Fig. 2.** (A) Stereo view of the binding site for the tyrosine residue in the EGFR internalization signal FYRALM, showing part of the experimental electron density map, with phases calculated using the peptide complex data as native with the Xe and EMTS derivatives, and solvent flattening with a 70% solvent content. The peptide is represented with magenta bonds, and the residues at the top right with green bonds come from the other subunit in the crystallographic dimer. (B) Stereo view of the binding site for the TGN38 internalization signal DYQRLN, in the same view as (A). The difference electron density shown was calculated using the model from the FYRALM peptide structure with the peptide removed; density for the arginine in the Y+2 position is clearly visible, packed against Trp<sup>421</sup>. [Drawn with BOBSCRIPT (32)]

AP2 complexes has been suggested by the observation that they bind in a 1:1 molar ratio with ligand-activated, and therefore dimeric, EGFRs (24). Binding of dimeric receptors to AP2 dimers, which in turn bind multimers of clathrin, provides an implicit mechanism for the formation of the clathrin lattice. The position of the peptide binding sites in the groove of the dimer predicts that the internalization signal must be presented as an accessible region without defined secondary structure, which is in agreement with the observation that EGFR binding to AP2 is increased by the presence of urea (23).

The striking positive electrostatic potential of the  $\mu 2$  dimer may reflect an ability to interact with negatively charged moieties, including proteins (for example, the domain after the internalization signal in EGFR) or the head

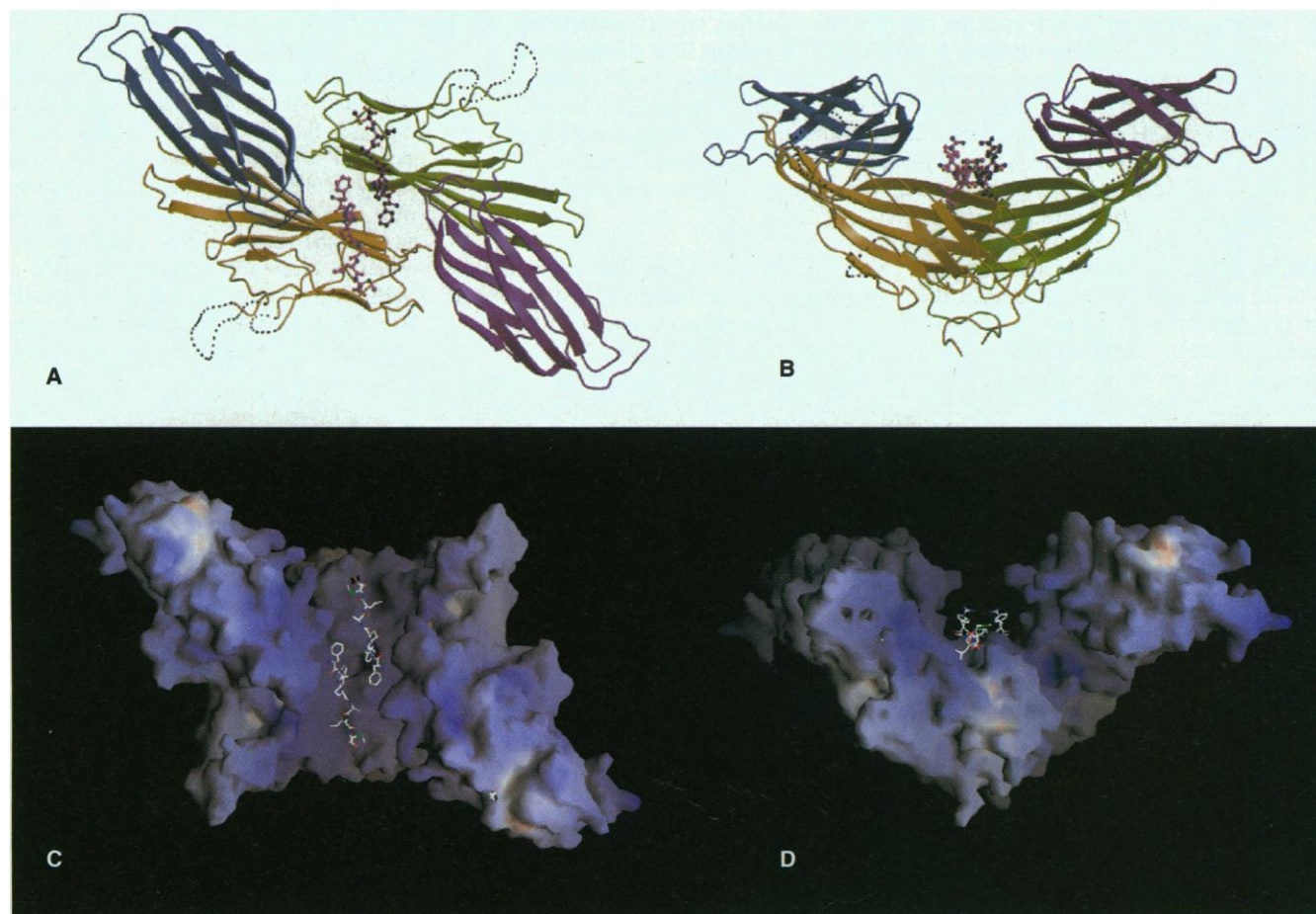
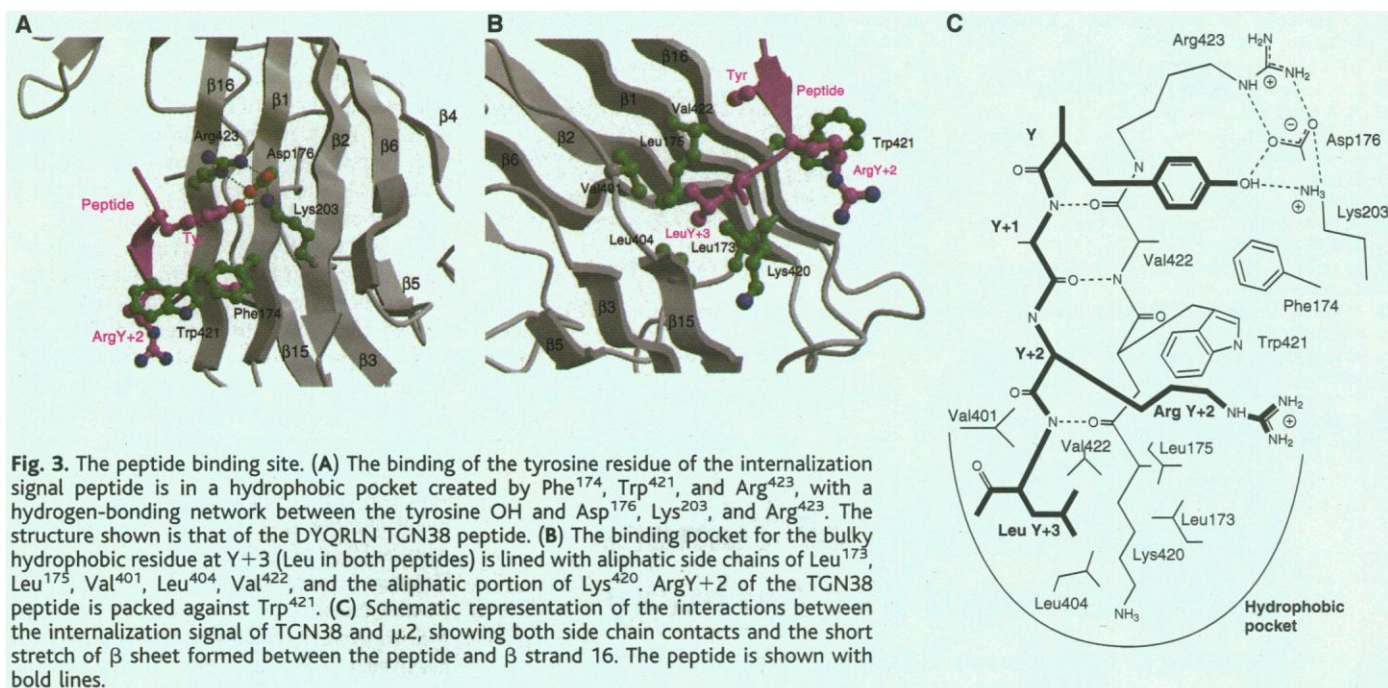
groups of negatively charged phospholipids such as phosphatidylserine. The planar face (Fig. 4D, top) would provide a large nonspecific ionic interaction with the membrane—which would increase the strength of binding to membrane proteins containing appropriately positioned internalization signals in a manner similar to proteins such as Src and HIV-1 gag (25)—and may also contribute in recruiting AP2 complexes to the plasma membrane.

The novel structure of the  $\mu 2$  subunit of the plasma membrane AP2 complexed with the FYRALM and DYQRLN peptides explains the specific binding of Yxx $\Phi$  internalization motifs and the absolute requirement for the motif to be in an extended  $\beta$ -strand conformation and for the tyrosine residue to be nonphosphorylated. The dimeric packing of the molecules in the crystal suggests that

the strength and selectivity of binding of receptors may be enhanced by their binding as dimers to dimeric  $\mu$  subunits.

References and Notes

1. T. Kirchhausen, J. S. Bonifacio, H. Riezman, *Curr. Opin. Cell Biol.* **9**, 488 (1997).
2. J. Schlessinger and A. Ullrich, *Neuron* **9**, 383 (1992).
3. W. S. Chen *et al.*, *Cell* **59**, 33 (1989).
4. A. Wells *et al.*, *Science* **247**, 962 (1990).
5. S. L. Schmid, *Annu. Rev. Biochem.* **66**, 511 (1997).
6. P. Wigge and H. T. McMahon, *Trends Neurosci.* **21**, 339 (1998).
7. W. Boll *et al.*, *EMBO J.* **15**, 5789 (1996).
8. H. Ohno *et al.*, *Science* **269**, 1872 (1995).
9. Abbreviations for the amino acid residues are as follows: A, Ala; C, Cys; D, Asp; E, Glu; F, Phe; G, Gly; H, His; I, Ile; K, Lys; L, Leu; M, Met; N, Asn; P, Pro; Q, Gln; R, Arg; S, Ser; T, Thr; V, Val; W, Trp; and Y, Tyr.
10. I. Rapoport, Y. Chen, C. P. Cupers, S. E. Shoelson, T. Kirchhausen, *EMBO J.* **17**, 2148 (1998).
11. M. Foti *et al.*, *J. Cell Biol.* **139**, 37 (1997).
12. S. Grzesiek, S. J. Stahl, P. T. Wingfield, A. Bax, *Biochemistry* **35**, 10256 (1996).
13. Residues 122 to 435 or 158 to 435 (TGN38 peptide complex) of rat  $\mu 2$  adaptin were expressed in *Escherichia coli* as an NH<sub>2</sub>-terminal H<sub>6</sub> fusion protein and were purified by Ni-NTA agarose and S200 gel filtration. Crystals were grown by hanging-drop vapor diffusion at 16°C against a reservoir containing 2.2 M NaCl, 0.4 M Na/K phosphate, 10 mM dithiothreitol, 15% (v/v) glycerol, and 0.1 M MES (pH 6.5 to 7.1) over a period of 2 weeks. Crystals of the complex with the synthetic hexapeptides FYRALM or DYQRLN were grown under similar conditions with a threefold molar ratio of peptide to protein. The crystals belong to space group P6<sub>3</sub> (unit cell  $a = b = 125.7$  Å,  $c = 73.2$  Å) with a single molecule in the asymmetric unit. All data were collected at 100 K at SRS Daresbury, station 9.6 (native, Xe, and Hg derivatives; DYQRLN complex,  $\lambda = 0.87$  Å) and station 7.2 (FYRALM complex,  $\lambda = 1.488$  Å), integrated with MOSFLM (26), and scaled with CCP4 programs (27) (Table 1). Despite the weak diffraction beyond 3 Å resolution, the high redundancy of the data gives significant information for the two peptide complexes to 2.7 Å. The structure was solved using a single-site xenon derivative (incubated at 7 bar for 10 min, then frozen quickly after releasing the pressure) and a mercury derivative [soaked in 10 mM ethyl mercury thiosalicylate (EMTS) for 30 min]. The sites were determined from difference Pattersons, and refinement and phasing were performed with SHARP (28), followed by solvent flattening with SOLOMON (29), using a solvent content of 70%. The initial model was built with O (30) to the map for the native data set at 3.0 Å resolution, then transferred to the higher resolution data set for the FYRALM complex and refined with REFMAC (31). The model of this complex includes the bound peptide and 51 water molecules, but is missing the first 44 residues (MH<sub>6</sub> tag and residues 122 to 158) as well as two loops, residues 221 to 237 and 256 to 260, for which there is no interpretable density. The native structure also contains electron density in the peptide binding site, probably from binding of an unidentified part of the NH<sub>2</sub>-terminus, so the derivatives were sufficiently isomorphous to the peptide complex to be used in phase calculations (Fig. 2A). The shorter construct (residues 158 to 435) used for the DYQRLN peptide complex did not crystallize in the absence of peptide; this isomorphous complex was refined starting with a model of the first complex with the peptide removed (Fig. 2B). Although the R factors are rather high, presumably because of the high overall B factor and the disordered regions, the experimental maps and the details of the peptide binding are clear (Fig. 2). The coordinates and structure factors have been deposited in the Protein Data Bank with codes 1BW8 (EGFR peptide complex) and 1BXX (TGN38 complex).
14. A. Sorkin, M. Mazzoti, T. Sorkina, L. Scotto, L. Beguinot, *J. Biol. Chem.* **271**, 13377 (1996).
15. K. Bos, C. Wraight, K. K. Stanley, *EMBO J.* **12**, 2219 (1993).



16. J. S. Humphrey, P. J. Peters, L. C. Yuan, J. S. Bonifacino, *J. Cell Biol.* **120**, 1123 (1993).  
 17. J. F. Collawn *et al.*, *Cell* **63**, 1061 (1990).  
 18. E. D. Lowe *et al.*, *EMBO J.* **16**, 6646 (1997).  
 19. M.-P. Egloff *et al.*, *ibid.*, p. 1876.  
 20. H. Ohno, M.-C. Fournier, G. Poy, J. S. Bonifacino, *J. Biol. Chem.* **271**, 29009 (1996).  
 21. Z. Songyang *et al.*, *Cell* **72**, 767 (1993).  
 22. G. Waksman *et al.*, *Nature* **358**, 646 (1992).  
 23. A. Nesterov, R. C. Kurten, G. N. Gill, *J. Biol. Chem.* **270**, 6320 (1995).  
 24. A. Sorkin, T. McKinsey, W. Shih, T. Kirchhausen, G. Carpenter, *ibid.*, p. 619.  
 25. D. Murray, N. Ben-Tal, B. Honig, S. McLaughlin, *Structure* **5**, 985 (1997).  
 26. A. G. W. Leslie, in *Joint CCP4 and ESF-EACMB Newsletter on Protein Crystallography No. 26* (SERC, Daresbury Laboratory, Warrington, UK, 1992).  
 27. Collaborative Computational Project, *Acta Crystallogr.* **D50**, 760 (1994).  
 28. E. de la Fortelle and G. Bricogne, *Methods Enzymol.* **276**, 472 (1997).  
 29. J. P. Abrahams and A. G. W. Leslie, *Acta Crystallogr.* **D52**, 30 (1996).  
 30. T. A. Jones, J. Y. Zou, S. W. Cowan, M. Kjeldgaard, *ibid.* **A47**, 110 (1991).  
 31. G. N. Murshudov, A. A. Vagin, E. J. Dodson, *ibid.* **D53**, 240 (1997).  
 32. R. M. Esnouf, *J. Mol. Graphics* **15**, 133 (1997).  
 33. A. Nicholls, K. A. Sharp, B. Honig, *Proteins* **11**, 281 (1991).  
 34. K. Diederichs and P. A. Karplus, *Nature Struct. Biol.* **4**, 269 (1997).  
 35. We thank M. S. Robinson for the rat  $\mu 2$  clone, A. J. McCoy and the staff of SRS Daresbury for assistance in data collection, L. LoConte and J. Janin for the surface area calculations, and H. T. McMahon, M. S. Robinson, and M. E. M. Noble for discussions.

12 August 1998; accepted 12 October 1998

## Reovirus Therapy of Tumors with Activated Ras Pathway

Matthew C. Coffey, James E. Strong, Peter A. Forsyth, Patrick W. K. Lee\*

Human reovirus requires an activated Ras signaling pathway for infection of cultured cells. To investigate whether this property can be exploited for cancer therapy, severe combined immune deficient mice bearing tumors established from *v-erbB*-transformed murine NIH 3T3 cells or human U87 glioblastoma cells were treated with the virus. A single intratumoral injection of virus resulted in regression of tumors in 65 to 80 percent of the mice. Treatment of immune-competent C3H mice bearing tumors established from *ras*-transformed C3H-10T1/2 cells also resulted in tumor regression, although a series of injections were required. These results suggest that, with further work, reovirus may have applicability in the treatment of cancer.

Activating mutations of the proto-oncogene Ras occur in about 30% of all human tumors (1), primarily in pancreatic (90%), sporadic colorectal (50%), and lung (40%) carcinomas and myeloid leukemia (30%). Because Ras is a key regulator of mitogenic signals, aberrant function of upstream elements such as receptor tyrosine kinases (RTKs) can also result in Ras activation in the absence of mutations in Ras itself (2). Indeed, overexpression of RTKs such as HER2/Neu/ErbB2 or the epidermal growth factor receptor (EGFR) is common in breast cancer (25 to 30%) (3), and overexpression of platelet-derived growth factor receptor (PDGFR) or of wild-type or truncated EGFR is prevalent in gliomas and glioblastomas (40 to 50%), tumor types in which Ras mutations are rare (4-6). At-

tempts to target the Ras signaling pathway for cancer therapy have focused on drugs such as farnesyltransferase inhibitors that down-regulate the pathway (7). In contrast, the possibility of exploiting the activated Ras pathway itself as an anticancer therapy has not been explored.

The human reovirus is a ubiquitous, non-enveloped virus containing 10 segments of double-stranded RNA as its genome (8). Reovirus infections in humans are believed to be mild and restricted to the upper respiratory and gastrointestinal (GI) tracts, but in general they are asymptomatic (8). Recent *in vitro* studies have shown that mouse fibroblasts that are resistant to reovirus infection become susceptible after transfection with the gene encoding EGFR (9) or with the *v-erbB* oncogene (10). Transformation of the reovirus-resistant NIH 3T3 cells with activated Sos or Ras also results in enhanced infection (11), indicating that an activated Ras signaling pathway is exploited by reovirus. Restriction of reovirus replication in untransformed NIH 3T3 cells is due to activation of the double-stranded RNA-activated protein kinase (PKR) by early viral transcripts, which in turn inhibits the translation of these transcripts (11). Activated Ras (or an

activated element of the Ras pathway) presumably inhibits (or reverses) PKR activation, thereby allowing viral protein synthesis. The selective replication of reovirus in cells with an activated Ras signaling pathway (11), coupled with the relatively nonpathogenic nature of this virus in humans (8), makes it attractive as a potential oncolytic agent.

To test the efficacy of reovirus as a tumor therapy, we implanted severe combined immune deficient (SCID) mice with *v-erbB*-transformed NIH 3T3 cells (designated THC-11), which support reovirus replication *in vitro* (10). Tumor cells were introduced subcutaneously and unilaterally into the hind flank of the mice. Palpable tumors (mean area of 0.31 cm<sup>2</sup>) were established after 2 weeks, and eight mice, each with one tumor, were given a single intratumoral injection of 1.0 × 10<sup>7</sup> plaque-forming units (PFUs) of reovirus serotype 3 (strain Dearing) in phosphate-buffered saline (PBS). Control tumors (*n* = 10 mice) were injected with equivalent amounts of ultraviolet (UV)-inactivated virus. The single dose of reovirus resulted in marked (~80%) repression of tumor growth in six of eight animals by day 12 (Wilcoxon test: *P* = 0.0062) (Fig. 1) when tumors in the control animals exceeded the acceptable tumor burden.

We next assessed the efficacy of reovirus against human tumor cells. We tested the human glioblastoma U87 cell line because it overexpresses the PDGFR (5, 12) and thus has increased levels of activated Ras (6). These cells were susceptible to reovirus infection *in vitro* as evidenced by the synthesis of viral proteins and shutoff of host protein synthesis within 24 hours after infection (Fig. 2A) and widespread cytopathic effects by 48 hours (Fig. 2B). The U87 cells were then implanted as xenografts into the hind flank of SCID mice.

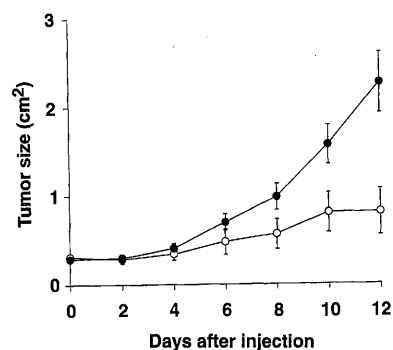


Fig. 1. Effect of reovirus on murine THC-11 tumors (*v-erbB*-transformed NIH 3T3 cells) grown subcutaneously in SCID mice (22). Each mouse received a single implant. Two weeks after implantation, tumors were injected with 1.0 × 10<sup>7</sup> PFUs of reovirus (open circles; *n* = 8 tumors) or an equivalent amount of UV-inactivated reovirus (filled circles; *n* = 10 tumors), and tumor growth was followed for 12 days. The experiment was repeated two additional times with similar results (mean ± SEM).

M. C. Coffey, J. E. Strong, P. W. K. Lee, Cancer Biology Research Group and Department of Microbiology and Infectious Diseases, University of Calgary Health Science Centre, Calgary, Alberta, T2N 4N1, Canada. P. A. Forsyth, Cancer Biology Research Group and Department of Oncology, University of Calgary Health Science Centre, Calgary, Alberta, T2N 4N1, Canada.

\*To whom correspondence should be addressed. E-mail: plee@acs.ucalgary.ca